Possible shape coexistence in odd-*A* Ne isotopes and the impurity effects of Λ hyperons[*]

Qian-Kun Sun(孙乾坤)[1]   Ting-Ting Sun(孙亭亭)[1†]   Wei Zhang(张炜)[1]

Shi-Sheng Zhang(张时声)[2]   Chen Chen(陈晨)[1,3]

[1]School of Physics and Microelectronics, Zhengzhou University, Zhengzhou 450001, China
[2]School of Physics and Nuclear Energy Engineering, Beihang University, Beijing 100191, China
[3]School of Nuclear Science and Technology, Lanzhou University, Lanzhou 730000, China

Abstract: In this study, shape evolution and possible shape coexistence are explored in odd-*A* Ne isotopes in the framework of the multidimensionally constrained relativistic-mean-field (MDC-RMF) model. By introducing s_Λ and p_Λ hyperons, the impurity effects on the nuclear shape, energy, size, and density distribution are investigated. For the *NN* interaction, the PK1 parameter set is adopted, and for the Λ*N* interaction, the PK1-Y1 parameter set is used. The nuclear ground state and low-lying excited states are determined by blocking the unpaired odd neutron in different orbitals around the Fermi surface. Moreover, the potential energy curves (PECs), quadrupole deformations, nuclear r.m.s. radii, binding energies, and density distributions for the core nuclei as well as the corresponding hypernuclei are analyzed. By examining the PECs, possibilities for shape coexistence in ^{27,29}Ne and a triple shape coexistence in ^{31}Ne are found. In terms of the impurity effects of Λ hyperons, as noted for even-even Ne hypernuclear isotopes, the s_Λ hyperon exhibits a clear shrinkage effect, which reduces the nuclear size and results in a more spherical nuclear shape. The p_Λ hyperon occupying the $1/2^-[110]$ orbital is prolate, which causes the nuclear shape to be more prolate, and the p_Λ hyperon occupying the $3/2^-[101]$ orbital displays an oblate shape, which drives the nuclei to be more oblate.

Keywords: hypernuclei, shape coexistence, impurity effects, Ne isotope

I. INTRODUCTION

In the extensive nuclide chart, most nuclei are observed to be deformed. In these nuclei, shape evolution and possible shape coexistence, which was first introduced by Morinaga in 1956 [1], have attracted considerable attentions. Later, Heyde and Wood revealed that shape coexistence is ubiquitous and may appear across the entire nuclide chart [2–4]. Moreover, triple and multiple shape coexistences have been observed or predicted [5, 6]. As one evidence of the appearance of shape coexistence, exploring the delicate interplay between the single-particle and collective behavior of nucleons, which exhibit opposite trends in nuclei, could promote understanding of nuclear collectivity and the nuclear shell structure [7].

Investigations on hypernuclear systems provide invaluable information for exploring many-body hadronic physics with "strangeness" utilized as a new degree of freedom [8–13]. In hypernuclei, hyperons have the advantage of being free from the Pauli exclusion principle for nucleons, and as a result, they can move deep into the nuclear interior as an impurity to probe nuclear structures and properties. Numerous studies have been performed on single-Λ hypernuclei both experimentally [14–17] and theoretically [18–24]. The interesting impurity effects of hyperons have been studied from various aspects, such as the nuclear size and binding energies [25, 26], nuclear cluster structures [18, 19, 27], neutron drip line [28–30], nucleon and hyperon skin or halo [30– 33], and pseudospin symmetry of nucleons [34].

The impurity effects of Λ hyperons may also be observed from drastic changes in nuclear shape and deformation. Various studies have shown that *s*-wave and *p*-wave hyperons have significantly different impurity effects. By including a spherical s_Λ hyperon, the deformation of nuclei can be reduced, and the corresponding core

nucleus becomes more spherical. For instance, as shown in Ref. [35], research using the axially deformed RMF model for $^{29}_{\Lambda}$Si and $^{13}_{\Lambda}$C revealed that the oblate nuclei ^{28}Si and ^{12}C became spherical after adding an s_{Λ} hyperon. A similar conclusion was obtained in Ref. [36], where the triaxially-deformed RMF model was used to study the potential energy surfaces $E \sim (\beta, \gamma)$, which found that the additional s_{Λ} hyperon drove the ground state of light C, Mg, and Si isotopes to a point with a small β and soft γ. In contrast with the s_{Λ} hyperon, a p_{Λ} hyperon exhibits strong polarization effects, which may enhance nuclear deformation [37]. In Ref. [38], the study using the deformed Skyrme-Hartree-Fock (DSHF) model showed that p_{Λ} hyperons in the $1/2^{-}[110]$ and $3/2^{-}[101]$ states had different effects on nuclear deformation, which resulted in more prolate and oblate nuclear shapes, respectively. In recent years, shape-driven effects induced by a valence nucleon(s) in high-spin states have been extensively researched [39–41]. The nucleon occupying the high-j and low-Ω orbital can cause the nucleus to be more prolate. A similar hyperon effect has been confirmed that polarizes nuclear shapes [37, 42].

To describe nuclear deformation with various shape degrees of freedom, it is better to reduce the symmetric restrictions imposed when solving the equations of motion. In CDFT, we can do this with a harmonic oscillator (HO) basis [43, 44] or three-dimensional lattice space [45–48]. Recently, Zhou *et al.* developed the multidimensionally constrained covariant density functional theories (MDC-CDFTs) [49–52], which can accommodate various shape degrees of freedom. They applied this model to a series of investigations on, for example, the fission barriers of actinides [50, 51, 53–56], nonaxial octupole Y_{32} correlation in $N = 150$ isotones [57], the third minima and triple-humped barriers in light actinides [58], and potential energy curves (PECs) in the superheavy nucleus ^{270}Hs [59]. Subsequently, by including Λ hyperons, the MDC-CDFTs have been extended to study hypernuclei. Shape evolution in the C, Mg, and Si isotopes and the possible polarization effects of the Λ hyperon [36], the superdeformed states in Ar isotopes [42], the $\Lambda\Lambda$ pairing correlations [60], and the new effective ΛN interactions [61] have been either studied or developed. Recently, we used the MDC-CDFTs to explore shape evolution and possible shape coexistence in even-even Ne isotopes [62]. By exploring the PECs, possibilities for shape coexistence were found in nuclei ^{24,26,28}Ne. Furthermore, the impurity effects of the s_{Λ} and p_{Λ} hyperons on the nuclear shape, size, and binding energies were studied.

In this paper, following our previous study in Ref. [62], shape evolution and possible shape coexistence in odd-A Ne isotopes are explored with the MDC-RMF model by including the blocking effect for the unpaired odd neutron and the impurity effects are investigated by adding a single-Λ hyperon occupying the lowest s or p orbitals. For shape coexistence in odd-A Ne isotopes, in Ref. [63], constrained RMF+BCS calculations with the NL075 force has been performed and possible shape coexistence was predicted in ^{25,27}Ne. The paper is organized as follows: In Sec. II, the MDC-RMF model for single-Λ hypernuclei including the blocking effect is briefly presented. In Sec. III, numerical details are provided. After the results and discussions in Sec. IV, a summary and perspectives are provided in Sec. V.

II. MODEL

In the meson-exchange MDC-RMF model for single-Λ hypernuclei, the covariant Lagrangian density is composed of two parts:

$$\mathcal{L} = \mathcal{L}_0 + \mathcal{L}_{\Lambda}, \tag{1}$$

where $\mathcal{L}_0$ is the standard RMF Lagrangian density for nucleons. For details, see Refs. [64–68]. In the case of the Lagrangian density for the Λ hyperon $\mathcal{L}_{\Lambda}$, considering the neutral and isoscalar particle properties, only couplings with scalar-isoscalar σ and vector-isoscalar ω mesons are included, and $\mathcal{L}_{\Lambda}$ is expressed as

$$\mathcal{L}_{\Lambda} = \bar{\psi}_{\Lambda} \left[i\gamma^{\mu}\partial_{\mu} - m_{\Lambda} - g_{\sigma\Lambda}\sigma - g_{\omega\Lambda}\gamma^{\mu}\omega_{\mu} \right] \psi_{\Lambda} + \frac{f_{\omega\Lambda\Lambda}}{4m_{\Lambda}} \bar{\psi}_{\Lambda} \sigma^{\mu\nu}\Omega_{\mu\nu}\psi_{\Lambda}, \tag{2}$$

where the mass of the Λ hyperon, $m_{\Lambda} = 1115.6$ MeV, the coupling constants of the Λ hyperon with the σ and ω meson fields, $g_{\sigma\Lambda}$ and $g_{\omega\Lambda}$, and the parameter $f_{\omega\Lambda\Lambda}$ in the tensor coupling term between the Λ hyperon and ω field, which is strongly related to small single-Λ spin-orbit splitting [69], constitute the ΛN interaction. The field tensor of the ω field, $\Omega_{\mu\nu} = \partial_{\mu}\omega_{\nu} - \partial_{\nu}\omega_{\mu}$.

In the framework of the RMF model, using the variational procedure, the Dirac equations for baryons as well as the Klein-Gordon equations for mesons and photons can be obtained under the mean-field and no-sea approximations. The Λ hyperon satisfies the following Dirac equation:

$$[\boldsymbol{\alpha} \cdot \boldsymbol{p} + \beta(m_{\Lambda} + S_{\Lambda}) + V_{\Lambda} + T_{\Lambda}]\psi_{\Lambda} = \epsilon\psi_{\Lambda}, \tag{3}$$

where $\boldsymbol{\alpha}$ and β are the Dirac matrices, and S_{Λ}, V_{Λ}, and T_{Λ} represent the scalar, vector, and tensor parts, respectively, of the mean-field potentials for the Λ hyperon,

$$S_{\Lambda} = g_{\sigma\Lambda}\sigma, \tag{4}$$

$$V_{\Lambda} = g_{\omega\Lambda}\omega, \tag{5}$$

$$T_{\Lambda} = -\frac{f_{\omega\Lambda\Lambda}}{2m_{\Lambda}}\beta(\boldsymbol{\alpha} \cdot \boldsymbol{p})\omega. \tag{6}$$

In odd-A nuclei, the blocking effect for the unpaired nucleon should be treated, which is of a crucial importance [70–72]. The ground state of an odd system is a one-quasiparticle state, and in the BCS approach, it could be described by the following wave function [70, 71]:

$$\hat{\alpha}_{k_1}^+ |\mathrm{BCS}\rangle = \hat{a}_{k_1}^+ \prod_{k>0, k \neq k_1} (u_k + v_k \hat{a}_k^+ \hat{a}_{\bar{k}}^+)|0\rangle, \qquad (7)$$

where $|\mathrm{BCS}\rangle$ is the BCS vacuum state, $\hat{\alpha}_{k_1}^+$ and $\hat{a}_{k_1}^+$ are the creation operators for the quasiparticle and single-particle, respectively, and k_1 denotes the blocked orbital occupied by the unpaired particle.

To determine the nuclear ground state and low-lying excited states in an odd-A nucleus, a variety of calculations are performed with the odd nucleon blocked in different single-particle states k around the Fermi surface. As a result, the state with the lowest total binding energy is considered the ground state, while others form the low-lying excited energy spectra.

To obtain potential energy curves (PECs), constraint calculations [70] with a modified linear constraint method [50, 51] are performed, which has been effectively demonstrated in MDC-RMF calculations compared to the quadratic constraint method [36]. The Routhian is calculated as

$$E' = \langle \hat{H} \rangle + \sum_{\lambda\mu} \frac{1}{2} C_{\lambda\mu} Q_{\lambda\mu}, \qquad (8)$$

where $\hat{H}$ is the RMF Hamiltonian, and $C_{\lambda\mu}$ are variables that change their values in different iteration steps as follows:

$$C_{\lambda\mu}^{(n+1)} = C_{\lambda\mu}^{(n)} + k_{\lambda\mu}\left(\beta_{\lambda\mu}^{(n)} - \beta_{\lambda\mu}\right), \qquad (9)$$

where $C_{\lambda\mu}^{(n+1)}$ and $C_{\lambda\mu}^{(n)}$ are values obtained in the $(n+1)$th and nth iterations, respectively, $\beta_{\lambda\mu}$ is the desired nuclear deformation, and $\beta_{\lambda\mu}^{(n)}$ is the calculated value in the nth iteration. Changes in $C_{\lambda\mu}$ and $\beta_{\lambda\mu}$ are linked by a constant $k_{\lambda\mu}$.

The intrinsic multipole moment $Q_{\lambda\mu}$ in Eq. (8) can be calculated with the vector density $\rho_V(\boldsymbol{r})$ and spherical harmonics $Y_{\lambda\mu}(\Omega)$ by

$$Q_{\lambda\mu} = \int \mathrm{d}^3 \boldsymbol{r} \rho_V(\boldsymbol{r}) r^\lambda Y_{\lambda\mu}(\Omega). \qquad (10)$$

Subsequently, with the multipole moment, the corresponding deformation parameter $\beta_{\lambda\mu}$ can also be calculated using

$$\beta_{\lambda\mu} = \frac{4\pi}{3BR^\lambda} Q_{\lambda\mu}, \qquad (11)$$

where $R = 1.2A^{1/3}$ fm is the radius of the nucleus, with A as the total number of nucleons, and B represents the number of protons, neutrons, Λ hyperons, or total baryons.

In an axially symmetric system, we only have the good quantum numbers of parity and the z component of the angular momentum. In this case, calculations with only a single-constraint on the quadrupole deformation β_2 will be performed.

III. NUMERICAL DETAILS

Shape evolution and possible shape coexistence are explored in odd-A Ne isotopes with $A = 19 - 33$ using the self-consistent MDC-RMF model. Moreover, the impurity effects of Λ hyperons occupying the s or p orbitals are investigated. As a continuation of our previous study on even-even Ne isotopes [62], the same numerical details are used.

In the RMF functional, the PK1 [73] parameter set is used for the NN interaction. For the ΛN interaction, the PK1-Y1 [74] parameter set is adopted, where the scalar-isoscalar coupling constant $g_{\sigma\Lambda} = 0.580 g_\sigma$ and vector-isoscalar coupling constant $g_{\omega\Lambda} = 0.620 g_\omega$, which were determined by fitting the experimentally observed single-Λ binding energies, and the tensor coupling constant $f_{\omega\Lambda\Lambda} = -g_{\omega\Lambda}$, which was determined by reproducing p_Λ spin-orbit splittings in $^9_\Lambda$Be and $^{13}_\Lambda$C.

To solve the RMF equations, an axially deformed harmonic oscillator (ADHO) basis [43, 44] is taken with the truncation parameters $N_{\mathrm{F}} = 14$ for fermion shells and $N_{\mathrm{B}} = 20$ for boson shells, as in Ref. [36]. With these parameters, the truncation error in the binding energy of the nucleus ^{26}Si is less than 30 keV.

In the mean-field approximation, the translational symmetry is broken. To remedy this, the following microscopic center-of-mass (c.m.) correction [75] is employed:

$$E_{\mathrm{c.m.}} = -\frac{1}{2M}\langle \hat{\boldsymbol{P}}^2 \rangle, \qquad (12)$$

where M is the total nuclear mass.

The BCS approach is used to treat the pairing effects with a finite-range separable pairing force [76–78].

$$V(\boldsymbol{r}_1 - \boldsymbol{r}_2) = -G\delta\left(\tilde{\boldsymbol{R}} - \tilde{\boldsymbol{R}}'\right) P(\tilde{r}) P(\tilde{r}') \frac{1 - \hat{P}_\sigma}{2}, \qquad (13)$$

where G is the strength of the pairing force, $\tilde{\boldsymbol{R}}$ and $\tilde{r}$ are the center of mass and relative coordinates between the paired particles, respectively, and $P(\tilde{r})$ is a Gaussian shaped function.

$$P(\tilde{r}) = \frac{1}{(4\pi a^2)^{3/2}} \mathrm{e}^{-\tilde{r}^2/a^2}, \qquad (14)$$

where a is the effective range of the pairing force. Here, the strength G and range a are taken as

$$G = 728.0 \, \text{MeV} \cdot \text{fm}^3, \quad a = 0.644 \, \text{fm}, \quad (15)$$

which can be used to obtain the same momentum dependency of the pairing gap in nuclear matter as that of the D1S Gogny force [76].

In Fig. 1, the binding energy per nucleon E/A, matter radius r_m, and quadrupole deformation β_2 in the ground states of Ne isotopes determined by unconstrained RMF calculations with the PK1 parameter set are compared with the available experimental data [79]. In general, good consistency with the experimental results is revealed, indicating that the choice of the PK1 parameter set for the description of Ne isotopes is suitable.
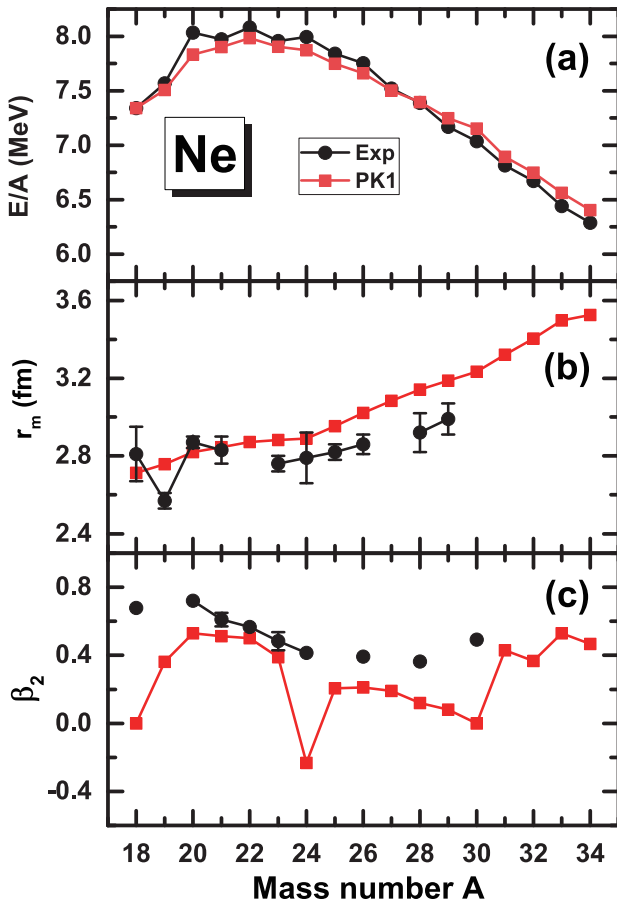
Fig. 1. (color online) Binding energy per nucleon E/A, matter radius r_m, and quadrupole deformation β_2 as a function of the mass number A in the ground states of Ne isotopes in comparison with the available experimental data [79].

IV. RESULTS AND DISCUSSIONS

To explore shape coexistence on the mean field level,

the PECs are mainly analyzed. If two close-lying energy minima with a difference of a few hundred keV that own prolate and oblate quadrupole deformations are observed in combination with a pronounced barrier between them, possible shape coexistence is indicated because their ground states may have two competing configurations.

In Fig. 2, the PECs for odd-A Ne isotopes from $A = 19$ to 33 are plotted as functions of the quadrupole deformation β_2, which are obtained using constrained calculations with the self-consistent MDC-RMF model. The unpaired odd neutron is blocked in different orbitals around the Fermi surface, and the state with the lowest binding energy is deemed the ground state while others form the local minima.

In Fig. 3, to observe the level structures in the Ne isotopes, the single-neutron levels $\Omega[Nn_3m_l]$ obtained using the constrained MDC-RMF calculations are plotted for the even-even nucleus ^{30}Ne, where the solid lines represent levels with positive parity, and the dashed lines represent those with negative parity. At a spherical shape with the deformation $\beta_2 = 0$, we observe the neutron shell closures $N = 8$ and $N = 20$, whereas the shell closure $N = 28$ vanishes owing to the inversion of the $1f_{7/2}$ and $2p_{3/2}$ levels. Referring to this single-neutron level structure, the odd neutron in $^{19-29}$Ne most likely occupies the $2s, 1d$ orbitals and $2p, 1f$ orbitals in ^{31,33}Ne. Calculations have been performed with all these configurations, and the obtained PECs are presented in Fig. 2, where the local energy minima are marked by open circles. The values of the quadrupole deformations, binding energies, and blocked orbitals of the unpaired odd neutron corresponding to the local energy minima are listed in Table 1.

Regarding the nucleus ^{19}Ne with a neutron number just exceeding an $N = 8$ shell closure, it is optimal that the odd neutron occupies the $1d_{5/2}$ orbital, which can be splitted into the $\Omega^\pi[Nn_3m_l] = 1/2^+[220]$, $3/2^+[211]$, and $5/2^+[202]$ orbitals with axially symmetric quadrupole deformation. Further analysis, shown in Fig. 2(a), demonstrates that the odd neutron blocked in the $1/2^+[220]$ orbital corresponds to the ground state with a prolate deformation of $\beta_2 = 0.361$, whereas the odd neutron blocked in $5/2^+[202]$ contributes to the second energy local minimum, which exhibits an oblate shape at $\beta_2 = -0.145$. In the case of the unpaired neutron occupying other orbitals, the obtained PECs (denoted by dashed lines) are significantly higher. Hereafter, we focus our attention on the configurations for the ground state and other local energy minima that may generate shape coexistence. With two more neutrons in ^{21}Ne, the odd neutron occupying the $3/2^+[211]$ orbital results in both the ground state and second local energy minimum, which are located at the prolate deformation of $\beta_2 = 0.512$ and oblate deformation of $\beta_2 = -0.201$, respectively. As for ^{23}Ne, the configurations of the ground state and the second local minimum are opposite to those in ^{19}Ne, that is, the odd neutron oc-
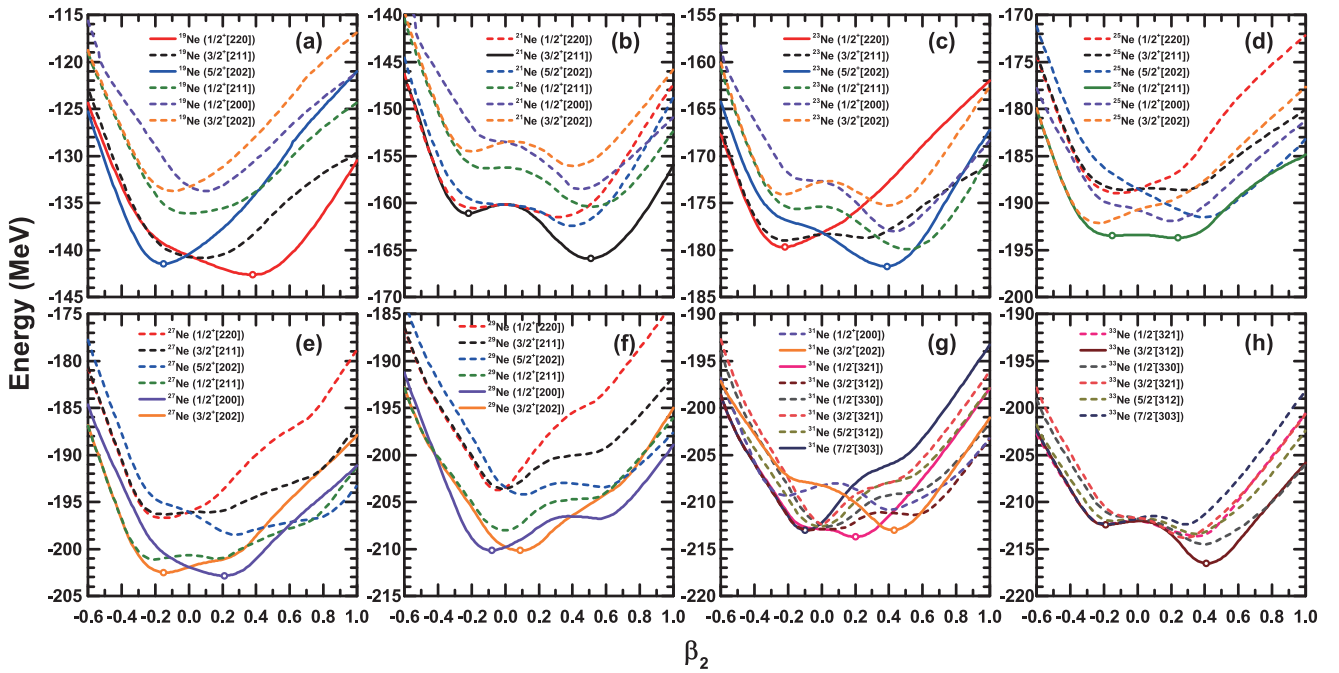
Fig. 2.   (color online) Potential energy curves (PECs) as a function of the deformation parameter β_2 in odd-*A* Ne isotopes, with the odd neutron blocked in different orbitals around the Fermi surface denoted by the Nilsson quantum numbers $\Omega^\pi[Nn_3m_l]$. The open circles denote local energy minima.
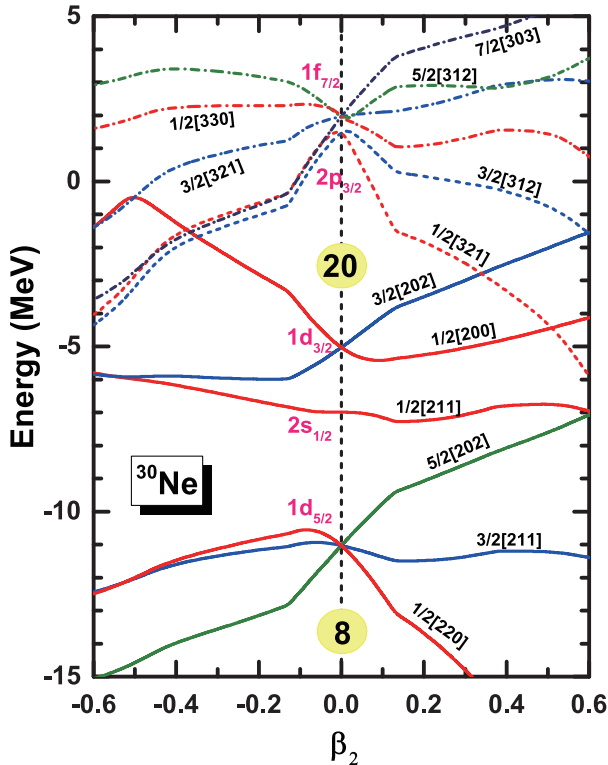

Fig. 3.   (color online) Single-neutron levels $\Omega[Nn_3m_l]$ as a function of the deformation parameter β_2 in ^{30}Ne.

cupying the $5/2^+$[202] orbital leads to the prolate ground state observed at $\beta_2 = 0.388$, while the odd neutron blocked in the $1/2^+$[220] orbital corresponds to the

second local energy minimum identified at the deformation $\beta_2 = -0.223$. Because the corresponding energy differences between the ground state and second local energy minimum in ^{19,21,23}Ne are as large as 1.135, 4.836, 2.058 MeV, possible shape coexistence is excluded in those nuclei. With regard to the nucleus ^{25}Ne, the configuration of the unpaired neutron blocked in $1/2^+$[211] from the spherical $2s_{1/2}$ orbital contributes to the lowest PEC, on which the ground state with the prolate deformation $\beta_2 = 0.206$ and the second local energy minimum with an oblate shape at $\beta_2 = -0.131$ are obtained. Although the energy difference between them is as small as 0.224 MeV, the circumjacent PEC is flat, where different deformations within a limited scope correspond to similar binding energies. In this case, the occurrence of shape coexistence is believed to be difficult. Moving further to the nuclei ^{27}Ne and ^{29}Ne, odd neutrons have great possibilities of occupying the $1d_{3/2}$ ($1/2^+$[200] and $3/2^+$[202]) orbital. For ^{27}Ne, when the odd neutron is blocked in the $1/2^+$[200] and $3/2^+$[202] orbitals, the ground state with prolate deformation at $\beta_2 = 0.190$ and second energy local minimum exhibiting an oblate shape at $\beta_2 = -0.130$ are observed, respectively. A small energy difference of 0.333 MeV in combination with a barrier of 0.984 MeV in height between them are observed, providing great potential for shape coexistence in ^{27}Ne. In the case of ^{29}Ne, with the odd neutron blocked in $3/2^+$[202], the prolate ground state is identified at a deformation of $\beta_2 = 0.080$, whereas the configuration with the odd neutron occupying $1/2^+$[200] leads to an oblate second local

Table 1. Quadrupole deformations and binding energies (in MeV) for ground states and local energy minima (labeled with asterisks) in $^{19-33}$Ne.

| Nucleus	Quadrupole deformation			Energy
	β_2	β_{2n}	β_{2p}	
^{19}Ne($1/2^+$[220])	0.361	0.303	0.413	−142.612
^{19}Ne*($5/2^+$[202])	−0.145	−0.138	−0.151	−141.477
^{21}Ne($3/2^+$[211])	0.512	0.515	0.509	−165.917
^{21}Ne*($3/2^+$[211])	−0.201	−0.209	−0.193	−161.081
^{23}Ne($5/2^+$[202])	0.388	0.370	0.411	−181.759
^{23}Ne*($1/2^+$[220])	−0.223	−0.236	−0.205	−179.701
^{25}Ne($1/2^+$[211])	0.206	0.193	0.225	−193.711
^{25}Ne*($1/2^+$[211])	−0.131	−0.131	−0.130	−193.487
^{27}Ne($1/2^+$[200])	0.190	0.177	0.213	−202.836
^{27}Ne*($3/2^+$[202])	−0.130	−0.135	−0.120	−202.503
^{29}Ne($3/2^+$[202])	0.080	0.068	0.103	−210.166
^{29}Ne*($1/2^+$[200])	−0.075	−0.073	−0.079	−210.144
^{31}Ne($1/2^-$[321])	0.191	0.196	0.181	−213.707
^{31}Ne*($7/2^-$[303])	−0.090	−0.089	−0.091	−213.022
^{31}Ne*($3/2^+$[202])	0.429	0.439	0.408	−212.986
^{33}Ne($3/2^-$[312])	0.419	0.428	0.397	−216.533
^{33}Ne*($3/2^-$[312])	−0.162	−0.182	−0.116	−212.418

minimum with a deformation of $\beta_2 = -0.075$. Similar to ^{27}Ne, owing to the small energy difference of 0.022 MeV coupled with a barrier of 0.4 MeV between the two local energy minima, possible shape coexistence is expected in ^{29}Ne. Far from the $N = 20$ shell closure, the unpaired neutron in the nuclei ^{31}Ne and ^{33}Ne is likely to occupy the $2p_{3/2}$ ($1/2^-$[321], $3/2^-$[312]) and $1f_{7/2}$ ($1/2^-$[330], $3/2^-$[321], $5/2^-$[312], $7/2^-$[303]) orbitals. For the nucleus ^{31}Ne, a possible triple shape coexistence is observed, which is comprised of the prolate ground state at $\beta_2 = 0.191$ with the odd neutron blocked in $1/2^-$[321], a second oblate local energy minimum at $\beta_2 = -0.090$ with the odd neutron in $7/2^-$[303], and a third prolate local minimum at $\beta_2 = 0.429$ with the odd neutron in $3/2^+$[202]. The corresponding excitation energies are 0.685 and 0.721 MeV with respect to the ground state, which together with a proper barrier between them, guarantees the appearance of shape coexistence. In the case of ^{33}Ne, with the odd neutron occupying $3/2^-$[312], both the ground state and the second local minimum are observed owing to a prolate shape at $\beta_2 = 0.419$ and an oblate shape at $\beta_2 = -0.162$, respectively. Because of the large energy difference of $\Delta E = 4.1$ MeV, the appearance of shape coexistence is difficult.

To explore the impurity effects of Λ hyperons, taking the single-Λ hypernucleus $^{28}_{\Lambda}$Ne (or denoted by ^{27}Ne$\otimes\Lambda$)

as an example, PECs are plotted in Fig. 4 where the *s*-wave ($\Omega^\pi[Nn_3m_l] = 1/2^+$[000]) and three *p*-wave ($1/2^-$[110], $1/2^-$[101], and $3/2^-$[101]) single-Λ hyperons are considered (denoted by dashed lines). In panels (a) and (b), the odd neutron is blocked in the $1/2^+$[200] and $3/2^+$[202] orbitals, respectively.

Generally, after injecting an s_Λ hyperon, the PEC shapes remain almost unchanged, while the depths deepen significantly owing to the attractive ΛN interaction. Moreover, a clear "glue-like" effect of the s_Λ hyperon is observed, which results in smaller nuclear deformations and a more spherical nuclear shape. For example, in Fig. 4(a), the reduced deformation of the prolate ground state changes from $\beta_2 = 0.190$ to $\beta_2 = 0.165$, and in Fig. 4(b), the deformation of the oblate second local minimum reduces to $\beta_2 = -0.115$ from $\beta_2 = -0.130$.

Regarding single-p_Λ hypernuclei, PECs obtained with the Λ hyperon injected into the $1/2^-$[101] orbital from the $1p_{1/2}$ orbital and the $3/2^-$[101] orbital from the $1p_{3/2}$ orbital are almost degenerate owing to small spin-orbit splitting; however, they exhibit significant differences from those obtained by injecting the p_Λ hyperon into the
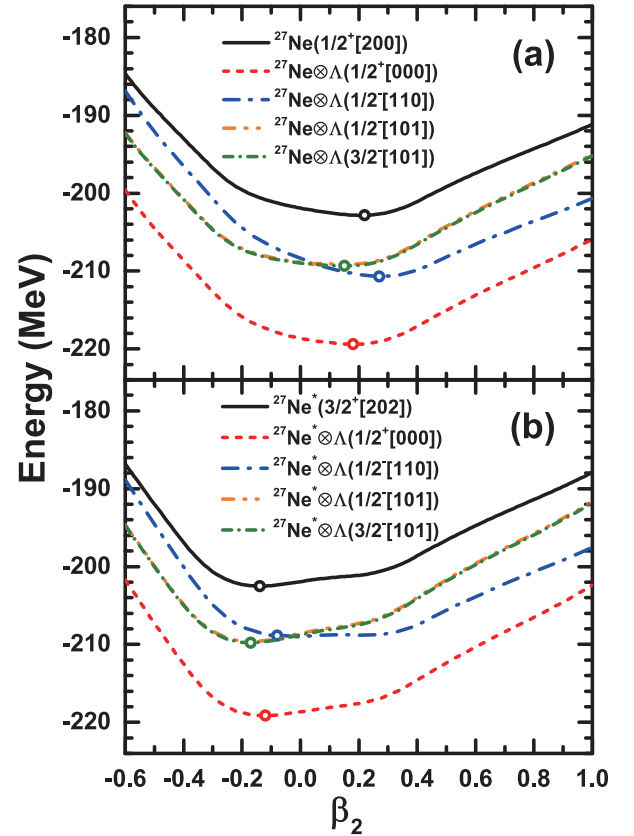
Fig. 4. (color online) PECs as a function of deformation β_2 in ^{27}Ne and the single-Λ hypernucleus $^{28}_{\Lambda}$Ne (^{27}Ne$\otimes\Lambda$). The odd neutron is blocked in the (a) $1/2^+$[200] and (b) $3/2^+$[202] orbitals, and the single-Λ hyperon is injected into the lowest *s* or *p* orbitals. The open circles denote the local energy minima.

$1/2^-[110]$ orbital. Hereafter, considering that the p_Λ hyperon occupying the $1/2^-[101]$ and $3/2^-[101]$ orbitals exhibit similar effects, we only discuss the latter case. In general, after injecting a p_Λ hyperon, the PEC shapes as well as the locations of the local energy minima clearly change. Furthermore, different polarization effects are exhibited by p_Λ hyperons occupying the $1/2^-[110]$ and $3/2^-[101]$ orbitals. For instance, in Fig. 4(a), with the Λ hyperon blocked in the $1/2^-[110]$ orbital, the prolate deformation of $\beta_2 = 0.190$ corresponding to the nuclear ground state in ^{27}Ne is driven to $\beta_2 = 0.265$, whereas it is reduced to $\beta_2 = 0.126$ when the p_Λ hyperon is blocked in the $3/2^-[101]$ orbital. Similar effects by the p_Λ hyperon have been observed in Fig. 4(b), where the unpaired neutron in the core nucleus is blocked in the $3/2^+[202]$ orbital, which corresponds to the second local minimum. In detail, the p_Λ hyperon in the $1/2^-[110]$ state drives the nucleus toward a spherical shape, and the oblate deformation of $\beta_2 = -0.130$ corresponding to the second local energy minimum decreases to $\beta_2 = -0.044$. Meanwhile, the p_Λ hyperon occupying the $3/2^-[101]$ orbital causes the hypernucleus to become more oblately deformed with $\beta_2 = -0.162$.

Similar investigations as those of $^{28}_{\Lambda}$Ne shown in Fig. 4 have also been performed for other Ne hypernuclei. The same impurity effects of single-Λ hyperons on nuclear deformations and binding energies are obtained. As a result of the introduced Λ hyperons, the nuclear PECs are significantly deepened; however, their increments are varied at different deformations β_2. Therefore, the energy difference ΔE between different local energy minima might change, which may influence the possibility of shape coexistence. In Table 2, the values of ΔE in the nuclei $^{19-33}$Ne are presented in comparison with values after injecting a single-Λ hyperon into the $1/2^+[000]$, $1/2^-[110]$, and $3/2^-[101]$ orbitals. With the additional s_Λ hyperon, the energy difference ΔE decreases significantly in all the hypernuclei. As a result, possible shape coexistence in ^{27,29,31}Ne can persist well in $^{28,30,32}_{\Lambda}$Ne. For example, the value of ΔE between the ground state and second local energy minimum reduces to 0.238 MeV in $^{28}_{\Lambda}$Ne from 0.333 MeV in ^{27}Ne. Moreover, the hypernucleus $^{20}_{\Lambda}$Ne becomes a new candidate for possible shape coexistence because ΔE therein is reduced to 0.924 MeV. With the addition of a p_Λ hyperon, the influence on the value of ΔE becomes complex. With the addition of a single-p_Λ hyperon occupying the $1/2^-[110]$ orbital, there is a significant increase in ΔE in all hypernuclei, which reduces the possibility of shape coexistence. For instance, the energy difference ΔE in $^{28}_{\Lambda}$Ne increases to 1.811 MeV from 0.333 MeV. Furthermore, one of the local energy minima disappears in $^{22,26}_{\Lambda}$Ne with the addition of a p_Λ hyperon. Similarly, by including a p_Λ hyperon in the state of $3/2^-[101]$, the values of ΔE increase in most of

Table 2. Energy difference ΔE (in MeV) between the two local energy minima in $^{19-33}$Ne (core nuclei) and the corresponding single-Λ hypernuclei $^{19-33}$Ne⊗Λ with the Λ hyperon injected into the $1/2^+[000]$, $1/2^-[110]$, and $3/2^-[101]$ orbitals.

	Core nuclei	$\Lambda(1/2^+[000])$	$\Lambda(1/2^-[110])$	$\Lambda(3/2^-[101])$
^{19}Ne⊗Λ	1.135	0.924	2.916	0.138
^{21}Ne⊗Λ	4.836	4.434	–	3.188
^{23}Ne⊗Λ	2.058	1.831	4.804	0.502
^{25}Ne⊗Λ	0.224	0.113	–	–
^{27}Ne⊗Λ	0.333	0.238	1.811	−0.443
^{29}Ne⊗Λ	0.022	0.020	0.902	−0.356
^{31}Ne⊗Λ	0.685	0.602	1.934	−0.019
^{33}Ne⊗Λ	4.115	3.955	6.218	2.834

the nuclei, and the probabilities of shape coexistence decrease. This differs from those in even-even Ne isotopes [62], where the additional p_Λ occupying the $3/2^-[101]$ orbital provides a higher possibility of shape coexistence.

To study the impurity effects of s_Λ and p_Λ hyperons on the nuclear quadrupole deformations β_2, nuclear root mean square (r.m.s.) radii r, and binding energies E, we take the hypernucleus $^{28}_{\Lambda}$Ne as an example and list the corresponding values in Table 3. The single-Λ separation energies $S_\Lambda = E(^{A+1}_{\Lambda}\text{Ne}) - E(^A\text{Ne})$ are also given. Configurations with the odd-neutron blocked in the $1/2^+[200]$ and $3/2^+[202]$ (denoted by asterisks) orbitals, which correspond to the ground state and the second local minimum of the core nucleus ^{27}Ne, are considered. In general, the s_Λ hyperon is more deeply bound than the p_Λ hyperon, which results in a relatively small nuclear size r_Λ and a large single-Λ separation energy S_Λ. Moreover, the s_Λ and p_Λ hyperons induce different impurity effects. The s_Λ hyperon exhibits a significant shrinkage effect, which makes the nuclei more bound with a smaller size. For example, with the addition of the s_Λ hyperon, the nuclear r.m.s. radius in the ground state ^{27}Ne($1/2^+[200]$) decreases from 3.083 fm to 3.074 fm, the total binding energy E becomes 16.546 MeV deeper, and the nuclear shape tends to be more spherical. For the quadrupole deformation β_2 of ^{27}Ne⊗Λ($1/2^+[000]$), it maintains the same sign as the core nucleus. In the case of the s_Λ hyperon, its deformation $\beta_{2\Lambda}$ is influenced in turn by the core nucleus. For instance, in the hypernucleus ^{27}Ne($1/2^+[200]$)⊗s_Λ, the Λ hyperon is slightly prolate with a deformation $\beta_{2\Lambda} = 0.053$, the sign of which is the same as that of the core nucleus ^{27}Ne($1/2^+[200]$). The same behavior is found in ^{27}Ne*($3/2^+[202]$)⊗s_Λ. In contrast with the s_Λ hyperon, the p_Λ hyperon may enhance the nuclear size slightly. Additionally, p_Λ hyperons in the states of $1/2^-[110]$ and $3/2^-[101]$ exhibit significantly different effects on nuclear deformation. For the p_Λ hyperon occupying $1/2^-[110]$, which is a prolate shape, the core

Table 3. Quadrupole deformation parameters, root mean square (r.m.s.) radii, binding energies, and Λ separation energies in the odd-A nucleus ^{27}Ne and the corresponding single-Λ hypernuclei ^{27}Ne$\otimes\Lambda$ with the Λ hyperon injected into the lowest s orbital or three p orbitals. The odd neutron is blocked in the $1/2^+$[200] and $3/2^+$[202] orbitals, which correspond to the ground state and the second local energy minimum (denoted by asterisks), respectively.

| Nucleus	Quadrupole deformation				r.m.s. radii/fm			Energy/MeV	
	β_2	β_{2n}	β_{2p}	$\beta_{2\Lambda}$	r_m	$r_{\rm core}$	r_Λ	E	S_Λ
^{27}Ne($1/2^+$[200])	0.190	0.177	0.213		3.083			-202.836	
^{27}Ne$\otimes\Lambda$($1/2^+$[000])	0.165	0.157	0.188	0.053	3.056	3.074	2.511	-219.382	16.546
^{27}Ne$\otimes\Lambda$($1/2^-$[110])	0.265	0.217	0.262	1.087	3.105	3.091	3.461	-210.693	7.857
^{27}Ne$\otimes\Lambda$($1/2^-$[101])	0.128	0.140	0.162	-0.414	3.093	3.079	3.443	-209.133	6.297
^{27}Ne$\otimes\Lambda$($3/2^-$[101])	0.126	0.138	0.161	-0.429	3.092	3.079	3.431	-209.317	6.481
^{27}Ne*($3/2^+$[202])	-0.130	-0.135	-0.120		3.077			-202.503	
^{27}Ne$^*\otimes\Lambda$($1/2^+$[000])	-0.115	-0.124	-0.109	-0.033	3.051	3.069	2.505	-219.144	16.641
^{27}Ne$^*\otimes\Lambda$($1/2^-$[110])	-0.044	-0.082	-0.061	0.774	3.088	3.075	3.432	-208.882	6.379
^{27}Ne$^*\otimes\Lambda$($1/2^-$[101])	-0.162	-0.155	-0.139	-0.509	3.094	3.080	3.444	-209.625	7.122
^{27}Ne$^*\otimes\Lambda$($3/2^-$[101])	-0.162	-0.154	-0.139	-0.530	3.094	3.080	3.439	-209.760	7.257

nucleus becomes more prolate. Conversely, for the hyperon occupying $3/2^-$[101] or $1/2^-$[101], which is oblate, the core nucleus becomes more oblate or less prolate. For instance, in ^{27}Ne($1/2^+$[200])$\otimes p_\Lambda$($1/2^-$[110]), because both the p_Λ hyperon and core nucleus are prolate, the p_Λ hyperon enhances the nuclear prolate deformation from $\beta_2 = 0.190$ to $\beta_2 = 0.265$, while shape decoupling occurs in ^{27}Ne($1/2^+$[200])$\otimes p_\Lambda$($3/2^-$[101]), where the p_Λ hyperon and core nucleus have different shapes, which leads to a reduction in the total nuclear deformation from $\beta_2 = 0.190$ to $\beta_2 = 0.126$. In Refs. [80, 81], shape decoupling in the deformed halo nuclei ^{42,44}Mg are discussed, in which the shapes of the core and outside halo are different.

In Fig. 5, the density distributions $\rho(r,z)$ in the r-z plane with the symmetric axis along the z-axis are shown for the nucleus ^{27}Ne (a) and the corresponding hypernucleus $^{28}_{\Lambda}$Ne (b,c,d). Cases with the core nucleus ^{27}Ne in the ground state and the second local minimum (denoted by asterisks) as well as the single-Λ hyperon occupying the $1/2^+$[000] (b), $1/2^-$[110] (c), and $3/2^-$[101] (d) orbitals are studied. In the upper and lower parts of panels (b–d), densities are plotted for the total hypernucleus and single-Λ hyperon, respectively. In Fig. 5(a), a prolate shape is observed for the ground state of ^{27}Ne, while an oblate shape is observed for the second energy minimum. After introducing an s_Λ hyperon, in Fig. 5(b), the nuclear shapes remain almost unchanged but with an increment of inner density. Meanwhile, the injected s_Λ hyperon is slightly deformed and has the same shape as the core nucleus. In Fig. 5(c), a "dumbbell" shape is observed for the prolate p_Λ hyperon in the state of $1/2^-$[110], the addition of which increases (reduces) the prolate (oblate) deforma-

tion of the core nucleus in the ground state (second energy minimum). At the same time, owing to the coupling of the p_Λ hyperon and nuclear core, slight differences in the density distributions of the p_Λ hyperon are observed in the two cases (panel c). In Fig. 5(d), a "ring" shape is observed for the oblate p_Λ hyperon in the state of $3/2^-$[101]. As a result, deformation of the prolate ground state decreases, and the oblate deformation of the second energy minimum is enhanced. A similar analysis of the impurity effects of the p_Λ hyperon on the nuclear density can be found in Refs. [38, 62].

To explain the mechanism behind the effects of s_Λ and p_Λ hyperons on nuclear densities and shapes in an intuitive way, taking ^{27}Ne$\otimes\Lambda$ with the core nucleus in the ground state an example, we present density distributions ρ along the r- and z-axes in Fig. 6. For the s_Λ hyperon, almost the same density distributions (red dashed lines in the lower part of each panel) are found along the r- and z-axes; however, the distribution is slightly extended along the z-axis, which suggests the s_Λ hyperon has a weakly prolate shape. With the addition of an s_Λ hyperon to ^{27}Ne, the nuclear density clearly increases in the inner part ($r < 3$ fm, $z < 2.5$ fm) both in the directions of the r- and z-axes. However, for the densities on the outer nuclear side, different influences are found, that is, $\rho(r)$ becomes slightly more extended while $\rho(z)$ shrinks. These cause ^{27}Ne$\otimes\Lambda$ to become more spherical compared to the core nucleus. In the case of the p_Λ hyperon occupying $1/2^-$[110], $\rho(r)$ vanishes and a visible distribution is presented along the z-axis with a maximum at $z = 2.5$ fm. As a result, a clear increment in the nuclear density along the z-axis is induced, and the nuclear shape becomes more prolate. For the p_Λ hyperon in the state of
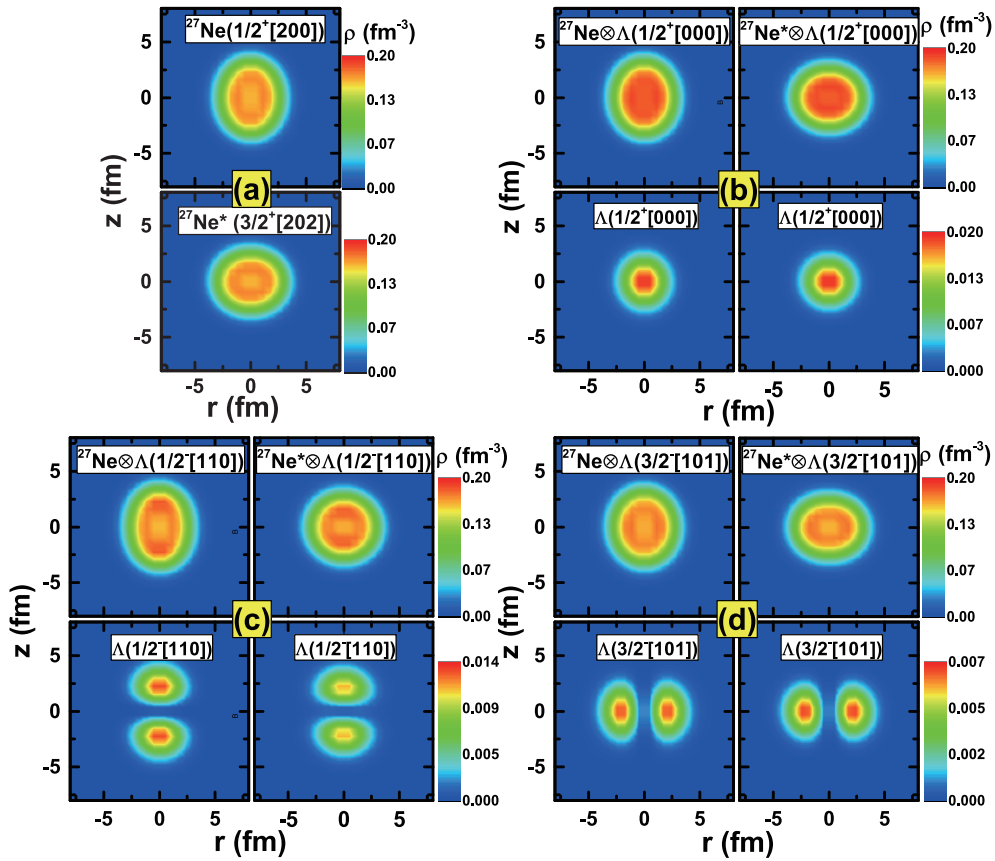
Fig. 5.   (color online) Two-dimensional density distributions in the *r-z* plane for (a) the core nucleus ^{27}Ne and (b), (c), (d) the corresponding single-Λ hypernuclei with the Λ hyperon injected into the (b) $1/2^+[000]$, (c) $1/2^-[110]$, and (d) $3/2^-[101]$ orbitals, respectively. The odd neutron in the ground state and the second local minimum (denoted by asterisks) occupies the $1/2^+[200]$ and $3/2^+[202]$ orbitals, respectively. The upper and lower parts of panels (b), (c), and (d) are the densities of the entire hypernuclei and the single-Λ hyperon, respectively.
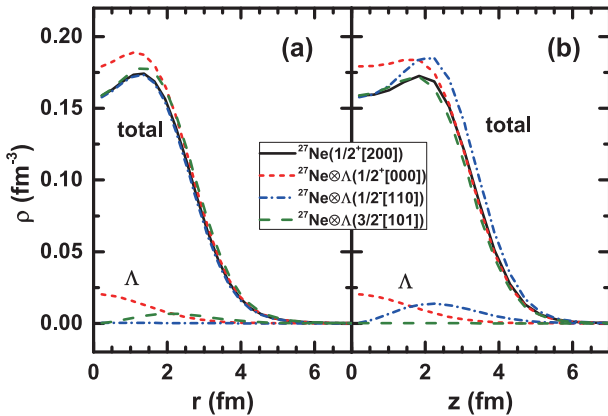
Fig. 6.   (color online) Density distributions $\rho(r,z)$ along the *r*-axis (a) and *z*-axis (b) in ^{27}Ne with the odd neutron occupying $1/2^+[200]$ (solid lines) and the corresponding single-Λ hypernuclei (dashed lines) with the Λ hyperon injected into the $1/2^+[000]$ (red short dashed line), $1/2^-[110]$ (blue dash-dotted line), and $3/2^-[101]$ (olive dashed line) orbitals. In the upper and lower parts of each panel, density distributions contributed by the total nuclei and the Λ hyperon are plotted, respectively.

$3/2^-[101]$, the nuclear density is enhanced in the direction of the *r*-axis and prolate deformation is weakened.

V. SUMMARY AND PERSPECTIVES

In this study, following our previous research [Sci. China-Phys. Mech. Astron. 64, 282011(2021)], shape evolution and possible shape coexistence in odd-*A* Ne isotopes are explored using the MDC-RMF model, which has achieved great success in describing nuclear deformations. Moreover, by introducing *s*- or *p*-wave Λ hyperons, the impurity effects on nuclear shape, energy, size, and density distribution are discussed. For *NN* and Λ*N* interactions in the RMF functional, the PK1 and PK1-Y1 parameter sets are adopted, respectively.

By blocking the unpaired odd neutron in different orbitals around the Fermi surface, the nuclear ground state and other local energy minima are determined, and by examining the PECs, possible shape coexistences in ^{27,29}Ne and a possible triple shape coexistence in ^{31}Ne are predicted. For ^{27}Ne, with the odd neutron blocked in the $1/2^+[200]$ and $3/2^+[202]$ orbitals, the ground state is ob-

served in a prolate shape at a deformation of $\beta_2 = 0.190$ and the second energy minimum exhibits an oblate shape at $\beta_2 = -0.130$, respectively. A small energy difference of 0.333 MeV and a barrier with a height of 0.984 MeV between them are observed, supporting possible shape coexistence in ^{27}Ne. Similarly, in ^{29}Ne, with the odd neutron blocked in the $3/2^+[202]$ orbital, the prolate ground state is identified at $\beta_2 = 0.080$, while the configuration with the odd neutron occupying $1/2^+[200]$ leads to an oblate second local minimum at $\beta_2 = -0.075$. In the case of ^{31}Ne, possible triple shape coexistence, including the ground state at $\beta_2 = 0.191$ with the odd neutron blocked at $1/2^-[321]$, the second local energy minimum at oblate deformation $\beta_2 = -0.090$ with the odd neutron at $7/2^-[303]$, and the third local minimum at prolate deformation $\beta_2 = 0.429$ with the odd neutron at $3/2^+[202]$, is predicated.

To discuss the impurity effects of s_Λ and p_Λ hyperons, nuclear quadrupole deformations, r.m.s. radii, binding energies, and density distributions are compared in detail for ^{27}Ne and the corresponding hypernuclei $^{28}_{\Lambda}$Ne in cases where the odd neutron occupies the $1/2^+[200]$ and $3/2^+[202]$ orbitals. The s_Λ hyperon exhibits clear shrinkage effects, which reduces the nuclear size and deformation. In contrast, the p_Λ hyperon exhibits strong polarization effects, which may enhance the nuclear deformation. Meanwhile, the p_Λ hyperons occupying different orbitals exhibit different effects: the hyperon from the $1/2^-[110]$

orbital drives the nuclear shape to become more prolate, and the hyperon in the $3/2^-[101]$ or $1/2^-[101]$ state results in a more oblate nuclear shape. These conclusions are consistent with those for even-even Ne isotopes [62]. Furthermore, with the addition of the s_Λ hyperon, the energy difference ΔE between the ground state and second local energy minimum decreases, which may increase the probability of shape coexistence. However, introducing a p_Λ hyperon results in a distinct disadvantage for shape coexistence in most of hypernuclei.

In the present study, we investigate shape evolution and possible shape coexistence at the mean-field level by analyzing PECs. This is the first step in our research. Recently, in Refs. [82, 83], the angular momentum and parity projected multidimensionally constrained relativistic Hartree-Bogoliubov model was developed. In the future, we aim to go beyond the mean-field to perform studies [84– 87]. Quantities such as electric quadrupole transitions $B(E2)$ will also be analyzed to study the shape coexistence and impurity effects of Λ hyperon, as conducted in Refs. [38, 88].

References

[1]   H. Morinaga, Phys. Rev. **101**, 254 (1956)

[2]   K. Heyde, P. Van Isacker, M. Waroquier, J. Wood, and R. Meyer, Phys. Rep. **102**, 291 (1983)

[3]   J. Wood, K. Heyde, W. Nazarewicz, M. Huyse, and P. Van Duppen, Phys. Rep. **215**, 101 (1992)

[4]   K. Heyde and J. L. Wood, Phys. Scr. **91**, 083008 (2016)

[5]   A. N. Andreyev, M. Huyse, P. Van Duppen *et al.*, Nature **405**, 430 (2000)

[6]   P. E. Garrett, T. R. Rodríguez, A. D. Varela *et al.*, Phys. Rev. Lett. **123**, 142502 (2019)

[7]   K. Wrzosek-Lipska and L. P. Gaffney, J. Phys. G: Nucl. Part. Phys. **43**, 024012 (2016)

[8]   O. Hashimoto and H. Tamura, Prog. Part. Nucl. Phys. **57**, 564 (2006)

[9]   A. Feliciello and T. Nagae, Rep. Prog. Phys. **78**, 096301 (2015)

[10] A. Gal, E. V. Hungerford, and D. J. Millener, Rev. Mod. Phys. **88**, 035004 (2016)

[11] T.-T. Sun, E. Hiyama, H. Sagawa *et al.*, Phys. Rev. C **94**, 064319 (2016)

[12] C.-J. Xia, G.-X. Peng, T.-T. Sun *et al.*, Phys. Rev. D **98**, 034031 (2018)

[13] T.-T. Sun, S.-S. Zhang, Q.-L. Zhang *et al.*, Phys. Rev. D **99**, 023004 (2019)

[14] M. Danysz and J. Pniewski, Lond. Edinb. Dubl. Phil. Mag. **44**, 348 (1953)

[15] G. C. Bonazzola, T. Bressani, E. Chiavassa *et al.*, Phys. Rev. Lett. **34**, 683 (1975)

[16] T. Hasegawa, O. Hashimoto, S. Homma *et al.*, Phys. Rev. C **53**, 1210 (1996)

[17] T. Nagae, Prog. Theor. Phys. Supp. **185**, 299 (2010)

[18] J.-M. Yao, Z.-P. Li, K. Hagino *et al.*, Nucl. Phys. A **868**, 12 (2011)

[19] K. Hagino, J.-M. Yao, F. Minato *et al.*, Nucl. Phys. A **914**, 151 (2013)

[20] *Relativistic Density Functional for Nuclear Structure*, edited by J. Meng, International Review of Nuclear Physics Vol. 10 (World Scientific, Singapore, 2016)

[21] S.-H. Ren, T.-T. Sun, and W. Zhang, Phys. Rev. C **95**, 054318 (2017)

[22] X.-Y. Xing, J.-N. Hu, and H. Shen, Phys. Rev. C **95**, 054310 (2017)

[23] T.-T. Sun, C.-J. Xia, S.-S. Zhang *et al.*, Chin. Phys. C **42**, 025101 (2018)

[24] Z.-X. Liu, C.-J. Xia, W.-L. Lu *et al.*, Phys. Rev. C **98**, 024316 (2018)

[25] T. Motoba, H. Bandó, and K. Ikeda, Prog. Theor. Phys. **70**, 189 (1983)

[26] E. Hiyama, M. Kamimura, K. Miyazaki *et al.*, Phys. Rev. C **59**, 2351 (1999)

[27] E. Hiyama, M. Kamimura, T. Motoba *et al.*, Prog. Theor. Phys. **97**, 881 (1997)

[28] D. Vretenar, W. Pöschl, G. A. Lalazissis *et al.*, Phys. Rev. C **57**, R1060 (1998)

[29] X.-R. Zhou, A. Polls, H.-J. Schulze *et al*., Phys. Rev. C **78**, 054306 (2008)
[30] H.-F. Lü, J. Meng, S.-Q. Zhang *et al*., Eur. phys. J. A **17**, 19 (2003)
[31] E. Hiyama, M. Kamimura, T. Motoba *et al*., Phys. Rev. C **53**, 2075 (1996)
[32] H.-F. Lü and J. Meng, Chin. Phys. Lett. **19**, 1775 (2002)
[33] Y. Zhang, H. Sagawa, and E. Hiyama, Phys. Rev. C **103**, 034321 (2021)
[34] W.-L. Lu, Z.-X. Liu, S.-H. Ren *et al*., J. Phys. G: Nucl. Part. Phys. **44**, 125104 (2017)
[35] M. T. Win and K. Hagino, Phys. Rev. C **78**, 054311 (2008)
[36] B.-N. Lu, E.-G. Zhao, and S.-G. Zhou, Phys. Rev. C **84**, 014328 (2011)
[37] M. Isaka, M. Kimura, A. Dote *et al*., Phys. Rev. C **83**, 044323 (2011)
[38] B.-C. Fang, W.-Y. Li, C.-F. Chen *et al*., Eur. Phys. J. A **56**, 11 (2020)
[39] E. S. Paul, R. Ma, C. W. Beausang *et al*., Phys. Rev. Lett. **61**, 42 (1988)
[40] X. H. Zhou, Y. B. Xing, M. L. Liu *et al*., Phys. Rev. C **75**, 034314 (2007)
[41] W. Nazarewicz, M. A. Riley, and J. D. Garrett, Nucl. Phys. A **512**, 61 (1990)
[42] B.-N. Lu, E. Hiyama, H. Sagawa *et al*., Phys. Rev. C **89**, 044307 (2014)
[43] Y. Gambhir, P. Ring, and A. Thimet, Ann. Phys. **198**, 132 (1990)
[44] P. Ring, Y. Gambhir, and G. Lalazissis, Comput. Phys. Commun. **105**, 77 (1997)
[45] Z. X. Ren, S. Q. Zhang, and J. Meng, Phys. Rev. C **95**, 024313 (2017)
[46] Z. X. Ren, S. Q. Zhang, P. W. Zhao *et al*., Sci. China-Phys. Mech. Astron. **62**, 112062 (2019)
[47] P. Ring, Sci. China-Phys. Mech. Astron. **62**, 112063 (2019)
[48] G. L. Long, Sci. China-Phys. Mech. Astron. **62**, 112061 (2019)
[49] S.-G. Zhou, Phys. Scr. **91**, 063008 (2016)
[50] B.-N. Lu, E.-G. Zhao, and S.-G. Zhou, Phys. Rev. C **85**, 011301 (2012)
[51] B.-N. Lu, J. Zhao, E.-G. Zhao *et al*., Phys. Rev. C **89**, 014323 (2014)
[52] J. Zhao, B.-N. Lu, E.-G. Zhao *et al*., Phys. Rev. C **95**, 014320 (2017)
[53] B.-N. Lu, J. Zhao, E.-G. Zhao *et al*., J. Phys. Conf. Ser. **492**, 012014 (2014)
[54] B.-N. Lu, J. Zhao, E.-G. Zhao *et al*., Phys. Scr. **89**, 054028 (2014)
[55] B.-N. Lu, J. Zhao, E.-G. Zhao *et al*., EPJ Web Conf. **38**, 05003 (2012)
[56] J. Zhao, B.-N. Lu, D. Vretenar *et al*., Phys. Rev. C **91**, 014321 (2015)
[57] J. Zhao, B.-N. Lu, E.-G. Zhao *et al*., Phys. Rev. C **86**, 057304 (2012)
[58] J. Zhao, B.-N. Lu, T. Nikšić *et al*., Phys. Rev. C **93**, 044315 (2016)
[59] X. Meng, B.-N. Lu, and S.-G. Zhou, Sci. China-Phys. Mech. Astron. **63**, 212011 (2019)
[60] Y.-T. Rong, P.-W. Zhao, and S.-G. Zhou, Phys. Lett. B **807**, 135533 (2020)
[61] Y.-T. Rong, Z.-H. Tu, and S.-G. Zhou, Phys. Rev. C **104**, 054321 (2021)
[62] C. Chen, Q.-K. Sun, Y.-X. Li *et al*., Sci. China-Phys. Mech. Astron. **64**, 282011 (2021)
[63] J.-G Chen, X.-Z. Cai, T.-T. Wang *et al*., Chin. Phys. **14**, 2444 (2005)
[64] B. D. Serot and J. D. Walecka, Adv. Nucl. Phys. **16**, 1 (1986)
[65] P.-G. Reinhard, Rep. Prog. Phys. **52**, 439 (1989)
[66] P. Ring, Prog. Part. Nucl. Phys. **37**, 193 (1996)
[67] D. Vretenar, A. Afanasjev, G. Lalazissis *et al*., Phys. Rep. **409**, 101 (2005)
[68] J. Meng, H. Toki, S.-G. Zhou *et al*., Prog. Part. Nucl. Phys. **57**, 470 (2006)
[69] B. K. Jennings, Phys. Lett. B **246**, 325 (1990)
[70] P. Ring and P. Schuck, *The nuclear many-body problem* (Springer Science & Business Media, 2004)
[71] L.-L. Li, J. Meng, P. Ring *et al*., Chin. Phys. Lett. **29**, 042101 (2012)
[72] T.-T. Sun, Z.-X. Liu, L. Qian *et al*., Phys. Rev. C **99**, 054316 (2019)
[73] W.-H. Long, J. Meng, N. Van-Giai *et al*., Phys. Rev. C **69**, 034319 (2004)
[74] X.-S. Wang, H.-Y. Sang, J.-H. Wang *et al*., Comm. Theor. Phys. **60**, 479 (2013)
[75] M. Bender, K. Rutz, P. G. Reinhard *et al*., Eur. Phys. J. A **7**, 467 (2000)
[76] Y. Tian, Z.-Y. Ma, and P. Ring, Phys. Lett. B **676**, 44 (2009)
[77] Y. Tian, Z.-Y. Ma, and P. Ring, Phys. Rev. C **80**, 024313 (2009)
[78] T. Nikšić, P. Ring, D. Vretenar *et al*., Phys. Rev. C **81**, 054318 (2010)
[79] M. Wang, W.J. Huang, F.G. Kondev *et al*., Chin. Phys. C **45**, 030003 (2021)
[80] S.-G. Zhou, J. Meng, P. Ring *et al*., Phys. Rev. C **82**, 011301 (2010)
[81] L.-L. Li, J. Meng, P. Ring *et al*., Phys. Rev. C **85**, 024312 (2012)
[82] K. Wang, and B.-N. Lu, Commun. Theor. Phys. **74**, 015303 (2022)
[83] Y.-T. Rong, and B.-N. Lu, arXiv: 2201.02114, (2022)
[84] H. Mei, K. Hagino, and J. M. Yao, Phys. Rev. C **93**, 011301 (2016)
[85] H. Xia, X. Wu, H. Mei *et al*., Sci. China-Phys. Mech. Astron. **62**, 42011 (2018)
[86] H. Mei, K. Hagino, J. M. Yao *et al*., Phys. Rev. C **90**, 064302 (2014)
[87] J.-M. Yao, H. Mei, K. Hagino *et al*., AIP Conf. Proc. **2130**, 020008 (2019)
[88] H. Sagawa, X. R. Zhou, X. Z. Zhang *et al*., Phys. Rev. C **70**, 054316 (2004)